International Journal of Mass Spectrometry 298 (2010) 119–127

Contents lists available at ScienceDirect

International Journal of Mass Spectrometry

journal homepage: www.elsevier.com/locate/ijms

Characterization of simple isomeric oligosaccharides and the rapid separation of glycan mixtures by ion mobility mass spectrometry

Jonathan P. Williams[a], Megan Grabenauer[b], Richard J. Holland[c], Catherine J. Carpenter[b], Mark R. Wormald[d], Kevin Giles[e], David J. Harvey[d], Robert H. Bateman[e], James H. Scrivens[c,*], Michael T. Bowers[b,**]

[a] Department of Chemistry, University of Warwick, Gibbet Hill Rd, Coventry, CV4 7AL, UK
[b] Department of Chemistry and Biochemistry, University of California, Santa Barbara, CA, 93106, USA
[c] Department of Biological Sciences, University of Warwick, Gibbet Hill Rd, Coventry, CV4 7AL, UK
[d] Oxford Glycobiology Institute, Department of Biochemistry, University of Oxford, South Parks Rd, Oxford, OX1 3QU, UK
[e] Waters MS Technologies Center, Manchester, M23 9LZ, UK

ARTICLE INFO

Article history:
Received 24 June 2009
Received in revised form 17 August 2009
Accepted 23 August 2009
Available online 28 August 2009

Keywords:
Ion mobility
Oligosaccharide
Glycan
Traveling wave

ABSTRACT

Ion mobility techniques, using both traveling wave-based technology and standard drift tube methods, along with molecular modeling were used to examine the gas-phase conformational properties of a series of isomeric oligosaccharides and hydrazine-released *N*-linked glycans from various sources. Electrospray ionization was used to generate H^+ and Na^+ adducts of oligosaccharides as well as Na^+ and $H_2PO_4^-$ adducts of released *N*-linked glycans. The ion mobility mass spectrometry techniques were used to separate the isomeric oligosaccharides and the glycan mixtures. Good agreement was obtained between the theoretical and measured collision cross-sections. Glycans common to each glycoprotein were observed to have the same arrival time distribution independent of their source. In some cases support for multiple isomers was observed which correlated well with evidence obtained, where possible, from other experimental techniques. The sensitivity of the traveling wave ion mobility spectrometry (TWIMS) technique, together with the rapid experimental timescale, reproducibility and high information content make this an attractive approach for the characterization of complex mixtures of glycans released from glycoproteins. Successful calibration of the TWIMS arrival times/cross-sections was demonstrated using data from the drift tube instrument.

1. Introduction

Glycosylation is the co- and post-translational attachment of carbohydrate structures to a protein backbone. The carbohydrate moieties of these glycoconjugates have many important roles in biological systems. These roles include protein folding, cell–cell recognition and protection from proteolysis [1]. Glycosylation is one of the most prevalent forms of covalent protein modification, occurring for approximately 50% of all proteins in eukaryotic systems. Mammalian and plant glycoproteins can be either *N*-linked or *O*-linked. In *N*-linked glycosylation, oligosaccharides bind to the amide nitrogen of asparagine side chains where the asparagine forms part of an Asn-Xxx-Ser(Thr) consensus sequence in which Xxx is any amino acid except proline. In *O*-linked glycosylation, they bind to the hydroxy oxygen of serine and threonine side chains. Addition of carbohydrate-containing glycosylphosphatidylinositol anchors to proteins to allow for membrane attachment can also be considered a special form of glycosylation.

Despite the importance of oligosaccharides in biological systems, structural determination of these molecules is an analytical challenge compared to other biomolecules. Not only do the constituent monosaccharides (and their stereochemistry) have to be identified, but also how they link together to form the polymer needs to be determined. Given that monosaccharides have multiple linkage sites and each site has two possible anomeric linkage configurations, oligosaccharide structure can be very complex [2]. With the help of chemical degradation, derivatization and mass spectral fragmentation, oligosaccharide structure can be elucidated. There are also practical motivations for advancing glycomic research. For example, the pharmaceutical industry makes increasing use of recombinant synthesis of proteins due to the reduced cost and increased quality over extraction and purification approaches [3]. Modern methods can incorporate post-translational modifications such as phosphorylation and glycosylation and there is a requirement for a rapid, sensitive, information-rich method to monitor

* Corresponding author.
** Corresponding author. Tel.: +1 805 893 2893; fax: +1 805 893 8703.
E-mail addresses: j.h.scrivens@warwick.ac.uk (J.H. Scrivens), bowers@chem.ucsb.edu (M.T. Bowers).

1387-3806/$ – see front matter © 2009 Elsevier B.V. All rights reserved.
doi:10.1016/j.ijms.2009.08.006

glycosylation in these systems for process optimization and quality control purposes.

Conventional mass spectrometry only takes advantage of mass separation and gives no direct information about three-dimensional shape. Ion mobility spectrometry-mass spectrometry (IMS–MS) uses not only traditional mass separation techniques, but also separates ions based on their shape as reflected by their mobility in an inert buffer gas. The method can, therefore, distinguish isomers with identical masses but different cross-sections. In traditional IMS–MS, a weak uniform electric field is applied across a drift tube to pull ions through a helium buffer gas. Compact isomers with higher mobilities exit the drift tube before more extended isomers that have lower mobilities. This drift tube ion mobility spectrometry (DTIMS) configuration allows for the measurement of a well-defined ion mobility and thus, using kinetic theory, determination of an ion's collision cross-section. Comparing experimental cross-sections to those of theoretical structures reveals information about the true gas-phase structures being observed experimentally. In the Bowers group, this method has been applied successfully to a number of biological systems, including DNA helices [4,5], G-quadruplexes [6–8] and the Alzheimer's peptides Aβ40 and Aβ42 [9–11]. Despite the fact that these biomolecules have undergone electrospray ionization (ESI) for transfer to the gas phase, evidence suggests that to a significant extent, solution-phase conformations are retained. This characteristic has also been observed by other mass spectrometry groups. Pioneering work by Last and Robinson [12] demonstrated "compelling evidence for preservation of tertiary structure under controlled conditions" and a review by Heck and van den Heuvel [13], describing the analysis of intact protein complexes by mass spectrometry, strongly supports this view.

The development of traveling wave ion mobility spectrometry (TWIMS) [14] has significantly increased sensitivity and speed in comparison with the traditional DTIMS device, allowing for the analysis of samples at biologically relevant concentrations. TWIMS has been integrated into a commercial quadrupole time-of-flight instrument, the Synapt HDMS System (Waters Corporation, UK) [15]. The Synapt operates with excellent reproducibility and mass accuracy, and is capable of providing a wealth of information, being able to achieve ion mobility spectrometry-tandem mass spectrometry (IMS–MS/MS) with the choice of performing collision-induced dissociation before or after mobility separation. The indirect route that the ions take in the TWIMS mobility separator means that, unlike in DTIMS, the correlation between ion transit time and ion mobility is not a simple inverse relationship and thus absolute collision cross-sections cannot be obtained directly from TWIMS measurements alone. It has been shown, however, that estimates of collision cross-sections can be obtained by reference to samples with known cross-sections [16–19], provided that the data is obtained under the same experimental conditions, i.e., mobility gas, gas pressure, wave velocity, wave height, pusher frequency and injection energy [20].

Ion mobility methods have previously been used to study oligosaccharides. DTIMS investigations have been used to obtain structures of several small sodiated sugars [21,22] and to demonstrate the separation capability for a number of carbohydrate isomers [23–25]. Clemmer and coworkers have lately used traditional IMS–MS to examine glycans released from ovalbumin [26]. Recent work from the group of Hill and coworkers [27] expands on previous research by describing the successful resolution of carbohydrate isomers with different anomeric configurations together with the use of adducts and variation of mobility gas to improve separation. Differential mobility spectrometry has been employed to study aggregate formation in the analysis of oligosaccharides [28]. Here we report the results of a combined DTIMS and TWIMS investigation of a range of oligosaccharides. The ability of the TWIMS method, coupled with MS and MS/MS approaches, to characterize carbohydrates released from a number of glycoproteins (Table 1) is explored. The structures of the carbohydrate moieties associated with each of these proteins have been previously studied by methods such as NMR and traditional mass spectrometry [29–32]. With standard analysis methods, structural characterization can only occur after some sort of chromatographic separation technique, such as HPLC, has been applied. Carbohydrates (glycans) released from the glycoproteins are readily separated by ion mobility in TWIMS. Common glycans (e.g., $Man_{5-7}GlcNAc_2$, where Man = mannose, GlcNAc = *N*-acetylglucosamine) were observed to have reproducible arrival time distributions independent of their source. This indicates that despite the presence of other species in a complex mixture arrival time measurements are reproducible. Tandem mass spectrometry experiments on components separated using ion mobility are also demonstrated and found to provide additional information regarding carbohydrate structure. The sensitivity of the TWIMS technique, together with the rapid experimental timescale, reproducibility and high information content make this an attractive approach for the characterization of complex mixtures in glycomic research.

Table 1
Glycans investigated in this study.

TWIMS–MS: glycans released from the following glycoproteins

Bovine ribonuclease B
Chicken ovalbumin
Porcine thyroglobulin, desialylated porcine thyroglobulin

DTIMS- and TWIMS–MS: penta- and hexasaccharides

Name (abbreviation)	Structure
B-pentasaccharide (B-PS)	Galα1–3Galβ1–4Glc 2 3 Fucα1 Fucα1
Iso-B-pentasaccharide (iso-B-PS)	Galα1–3Galβ1–3Glc 2 4 Fucα1 Fucα1
Lacto-*N*-fucopentaose I (LNFP I)	Galβ1–3GlcNAcβ1–3Galβ1–4Glc 2 Fucα1
Lacto-*N*-fucopentaose V (LNFP V)	Galβ1–3GlcNAcβ1–3Galβ1–4Glc 3 Fucα1
Lacto-*N*-difucohexaose I (LNDFH I)	Galβ1–3GlcNAcβ1–3Galβ1–4Glc 2 4 Fucα1 Fucα1
Lacto-*N*-difucohexaose II (LNDFH II)	Galβ1–3GlcNAcβ1–3Galβ1–4Glc 4 3 Fucα1 Fucα1

We also have examined a series of isomeric penta- and hexasaccharides (Table 1) using both the DTIMS and TWIMS techniques to evaluate the isomer separation capabilities of the two methods. In the DTIMS experiments, collision cross-sections for the sodiated oligosaccharides were obtained. By comparing these values with cross-sections of model structures acquired by molecular mechanics calculations, we were able to determine the gas-phase structures of these species. In addition, the DTIMS experimental cross-sections are compared to the TWIMS results.

2. Experiment

2.1. Ion mobility spectrometry-mass spectrometry (IMS–MS)

2.1.1. DTIMS–MS instrument

IMS–MS experiments at UC Santa Barbara were performed on a home-built spectrometer consisting of a nano-ESI source, an

Table 2
Optimized TWIMS separator parameters.

Sample	ESI mode	Gas pressure (mbar)	T-wave height (V)	T-wave velocity (m/s)
Released *N*-glycans	Positive	0.5	11	400
Released *N*-glycans	Negative	0.5	18	500
Isomeric carbohydrates	Positive	0.75	14	300

ion funnel, and a mobility drift tube followed by a quadrupole mass analyzer and detector [33]. Samples are introduced into the nano-ESI source by means of a metal coated borosilicate capillary (Proxeon, Odense, Denmark). The ions generated are transferred, via a metal capillary, to the ion funnel where they can be accumulated and pulsed into the drift tube. A weak uniform electric field is applied across the drift tube to pull ions through a helium buffer gas (at ~5–7 mbar). To measure arrival time distributions (ATDs), ions are pulsed from the funnel into the drift tube. Ions are separated by their mobility, with compact structures traveling faster than extended structures. Ions exit the drift tube and are mass analyzed and detected as a function of arrival time, t_A. To measure mobility (K_0), t_A for a particular ion is measured as a function of the drift voltage (V) applied to the drift tube (of known pressure p and length ℓ). As shown in Eq. (1), a plot of t_A versus p/V yields a straight line with a slope inversely proportional to K_0 and has a y-intercept equal to t_0, the amount of time the ions spend outside the drift tube.

$$t_A = \frac{\ell^2 T_0}{K_0 p_0 T}\frac{p}{V} + t_0 \quad (1)$$

In this equation, standard temperature (T_0 = 273.15 K) and pressure (p_0 = 1.013 bar) are used to obtain a mobility independent of drift tube temperature and pressure, i.e., the reduced mobility, K_0.

The mobilities obtained in this experiment can be used to calculate an ion's collision cross-section using the following relationship obtained from kinetic theory [34].

$$\sigma = \frac{3ze}{16N}\left(\frac{2\pi}{\mu kT}\right)^{1/2}\frac{1}{K_0} \quad (2)$$

Here z is the number of charges on the ion, e is the electronic charge, N is the buffer gas number density, μ is the reduced mass of the ion and buffer gas, k is the Boltzmann constant and T is temperature.

2.1.2. TWIMS–MS instrument

All TWIMS experiments were performed in a hybrid quadrupole-ion mobility-orthogonal acceleration time-of-flight (oa-ToF) mass spectrometer (Synapt HDMS, Waters Corporation, Manchester, UK). The instrument was equipped with a nano-ESI source and operated at a source temperature of 120 °C. The sample solutions were introduced into the source region of the instrument by means of metal coated borosilicate capillaries (Waters Corporation, Manchester, UK). The cone was optimized between 60 and 130 V for ESI-MS/MS experiments and the collision energy was optimized to fragment the ion of interest, typically 110 eV in positive and 70 eV for negative ESI mode. A detailed explanation of the Synapt HDMS technology has been described elsewhere [15]. The instrument is comprised of three traveling wave enabled stacked ion guides: trap, ion mobility separator and transfer. The trap ion guide is used to accumulate ions and releases these as ion packets into the ion mobility separator for mobility separation. The transfer ion guide is used to convey the mobility-separated ions to the oa-ToF mass analyzer. Ions were mass selected using the quadrupole prior to MS/MS experiments. All MS/MS experiments were performed after ion mobility separation in the transfer cell. Optimized TWIMS operating conditions are listed in Table 2. The variation observed in these parameters is due to the distinct nature of the samples used. The glycans were run as complex mixtures requiring a wider m/z range while the isomeric carbohydrates were run as pure compounds over a limited m/z acquisition range. The ToF analyzer recorded 200 orthogonal acceleration pushes (mass spectra) with the pusher period set to an appropriate value depending on m/z acquisition range. The total acquisition time for the data shown was combined and averaged over 2 min. The ToF analyzer was tuned in V-optic mode for an operating resolution of 7000 (FWHM). Mass spectra were acquired at a rate of one spectrum per second with an interscan delay of 100 ms. Data acquisition and processing were carried out using MassLynx™ (v4.1) software (Waters Corporation, Milford, MA, USA).

2.1.3. Materials

Bovine ribonuclease B, chicken ovalbumin and porcine thyroglobulin were purchased from Sigma Chemical Co. Ltd. (Poole, Dorset, UK). Ribonuclease B [30] and chicken ovalbumin [31,32] contain only neutral sugars. Thyroglobulin [29], contained both sialylated and neutral sugars. A desialylated version of thyroglobulin was generated using 10% acetic acid for 30 min at 80 °C. The glycans from these proteins were released with hydrazine [35] and dissolved in a mixture of H_2O/methanol (1:1; v/v) to a concentration between 10 and 25 pmol/μL for analysis using the Synapt instrument. For negative ion ESI, the solvent contained 0.5 mM ammonium phosphate.

The six oligosaccharides B-pentasaccharide, iso-B-pentasaccharide, lacto-*N*-fucopentaose I and V, and lacto-*N*-difucohexaose I and II were purchased from Sigma–Aldrich Company Ltd. (Poole, UK) and were dissolved in a mixture of H_2O/methanol (1:1; v/v) to a concentration of 10 pmol/μL for analysis using both the DTIMS–MS and Synapt instruments.

2.2. Molecular modeling

Theoretical modeling of the six oligosaccharides investigated with DTIMS–MS was done with the AMBER 8 package of molecular dynamics software [36] using the general AMBER force field. Using structures of the oligosaccharides built in Hyperchem [37], partial charges were calculated following the RESP procedure within AMBER with Gaussian 03 [38] and the 6-31G* basis set. A set of initial structures was created for each oligosaccharide by building the molecule in xleap, then varying the position of the sodium counter ion. A simulated annealing protocol was used to generate 150–200 low-energy candidate structures for each initial structure of the oligosaccharides. In this protocol an initial structure was subjected to 30 ps of molecular dynamics at 600 K followed by 10 ps of dynamics during which the temperature was lowered to 0 K. The resulting structure was then energy minimized, saved, and used as the starting structure for the next cycle. The collision cross-sections of these candidate structures were then calculated using the exact hard-sphere scattering and trajectory models developed by the Jarrold group [39,40]. For each oligosaccharide the average cross-sections of the lowest-energy families of structures, which for the systems considered in this work showed only minor structural deviations, were reported. Figures were prepared using the UCSF Chimera package [41].

3. Results and discussion

3.1. The rapid separation of chemically released N-linked glycans

The TWIMS-based approach offers a number of advantages for the analysis of a complex mixture of released glycans. These include high sensitivity, rapid analysis, no requirement for further sample preparation and the high information content of the experiment. In addition to mobility separation, mass spectral information (both MS and MS/MS) can be obtained. By using an established calibration approach, based on accepted rotationally averaged cross-sectional values obtained from conventional DTIMS experiments, estimated cross-sections can also be obtained. An attractive feature of IMS–MS is the millisecond timescale of ion separation in the gas phase. This dovetails well with the second timescale of liquid chromatography and the microsecond timescale of mass spectrometry data acquisition. The established technique for separating oligosaccharide mixtures is normal-phase high-performance liquid chromatography (HPLC) [42]. The IMS–MS approach can be used in a similar manner to HPLC for the rapid separation of these complex mixtures without prior HPLC separation. To this end, we have used the TWIMS–MS and TWIMS–MS/MS methods to investigate the *N*-linked glycans released from the set of well-studied glycoproteins listed in Table 1.

The bovine ribonuclease B system will serve as a representative example of the type of results we are able to achieve with our techniques. This protein is known to have one glycosylation site that releases a mixture of oligosaccharides with the formulae $Man_nGlcNAc_2$, $n = 5–9$. The glycan structures have been determined by NMR analysis [30]. The positive-ion ESI mass spectrum of these oligosaccharides (Fig. 1) [43] is dominated by sodiated glycan species, which is consistent with previously published spectra [44].

Fig. 2 shows the ATDs measured for the four largest sodiated glycan peaks in the ribonuclease B mass spectrum ($Man_nGlcNAc_2$, $n = 5–8$). The distributions represent a typical glycan separation for this instrument which can be achieved in <16 ms. Each distribution is dominated by a single large peak that shifts to longer arrival times as n increases. This is an expected result, given that the increased size of an ion decreases its mobility as it passes through the mobility separator. For $n = 5–7$, the ATD peaks broaden slightly as n increases. Again, this is expected since the more time ions spend traveling through the mobility separator, the larger the spread in their transit times becomes. The ATD peak for $n = 8$ is even broader than would be expected based on the trend for $n = 5–7$. This additional broadening could be due to the presence of $Man_8GlcNAc_2$ isomers. The NMR study by Fu et al. [30] indicates that both $Man_7GlcNAc_2$ and $Man_8GlcNAc_2$ released from ribonuclease B have three linkage isomers (as depicted in Figs. 1 and 2). It is not clear why the $n = 7$ ATD peak is not broader like the $n = 8$ peak, since $Man_7GlcNAc_2$ also has three isomers. It may be that cross-sections of the $n = 8$ isomers happen to be different enough to give a broader ATD, while it is not the case for the $n = 7$ isomers. The presence of conformers may also play a role, with differences in the $n = 7$ and 8 species resulting in a wider range of conformer cross-sections for the larger glycan.

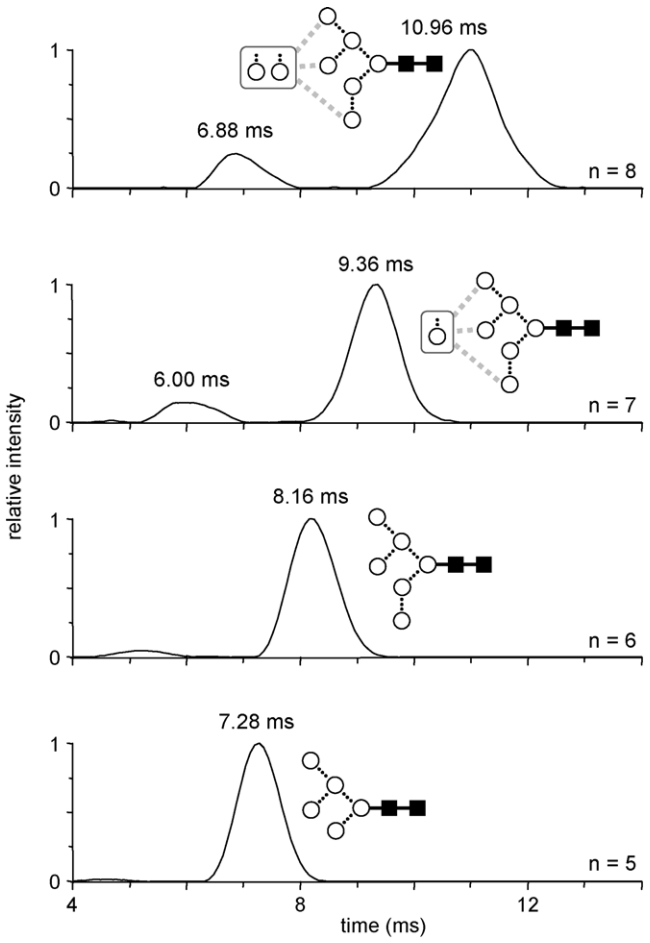

Fig. 2. TWIMS ATDs for the sodiated $Man_nGlcNAc_2$, $n = 5–8$ glycan mixture from ribonuclease B. Glycan structure labels follow key shown in Fig. 1. The small peaks at shorter times are doubly charged dimers.

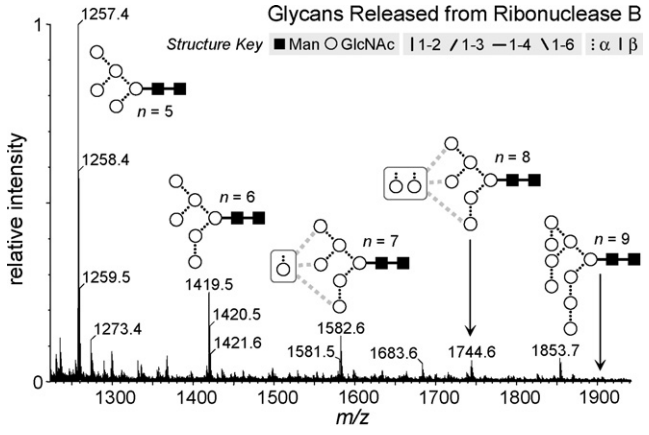

Fig. 1. Mass spectrum of sodiated $Man_nGlcNAc_2$ glycans released from ribonuclease B. Peaks are labeled with the corresponding unsodiated structure. The different linkages are distinguished by solid and dotted vertical, horizontal and diagonal lines [43].

Each ATD also has a small peak at shorter arrival times, for example, at 6.00 ms for $n = 7$ and 6.88 ms for $n = 8$, which are due to glycan dimers of the form $[2M+2Na]^{2+}$. This type of behavior has been observed before for the Alzheimer's peptides Aβ40 and Aβ42, where oligomers with the same m/z values as the monomer have shorter arrival times [9–11]. Oligomer-size assignments can be verified by measuring high-resolution mass spectra for each peak in the ATD. For example, Fig. 3 shows the mass spectrum obtained for the most prominent feature in the $Man_5GlcNAc_2$ ATD shown in Fig. 2. This ATD feature gives a ^{13}C isotope pattern with 1 Da spacings, unambiguously indicating a singly charged species, the monomer. Similarly, as has been shown for other systems [15], doubly charged dimers would give 0.5 Da spacings, triply charged trimers, 0.33 Da spacings, etc. The ability to obtain MS and MS/MS spectra for each ATD observed in the experiment is an important aspect of this instrument that allows significantly more confident assignment of the source of features in ATDs.

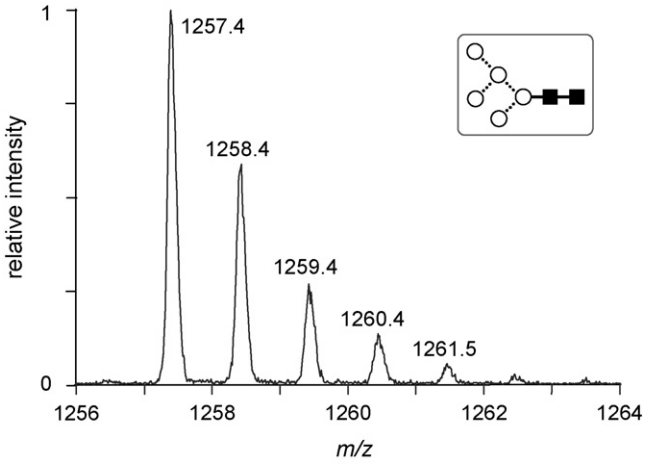

Fig. 3. Tandem mass spectrum obtained from the dominant peak in the $Man_5GlcNAc_2$ ATD shown in Fig. 2. Glycan structure labels follow key shown in Fig. 1.

3.2. Reproducibility of separation

To address whether the glycan source has an impact on the reproducibility of the separation, glycan $Man_5GlcNAc_2$ was released from four different sources: ribonuclease B, chicken ovalbumin, porcine thyroglobulin and desialylated thyroglobulin was studied with TWIMS. Fig. 4 shows ATDs for m/z 1257, the $[M+Na]^+$ ion, obtained from each source. The arrival times were 7.20–7.28 ms and reproducible to within one scan (±80 μs) for all experiments. The 1% difference between the top two distributions and the bottom two distributions is within experimental error. This demonstrates the independence of arrival time to other components within the complex glycan mixtures. All of the ATDs presented in this paper, from complex released glycan mixtures to isolated glycan standards, were reproducible to within one scan (±80 μs) over multiple experiments. This excellent reproducibility, combined with MS and MS/MS data provides high confidence in the ability to identify structures from ATDs.

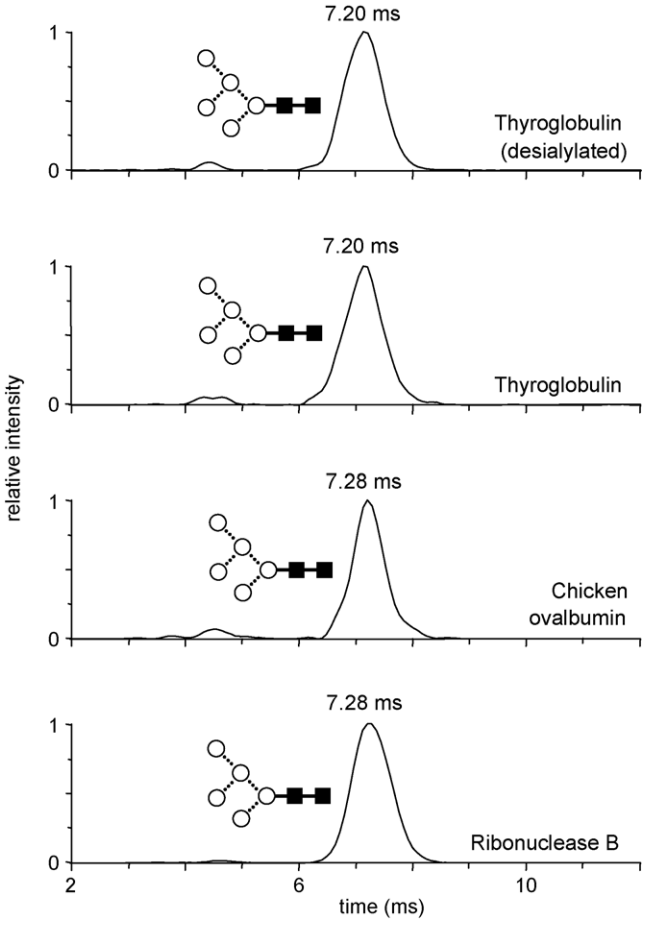

Fig. 4. TWIMS ATDs for sodiated $Man_5GlcNAc_2$ released from ribonuclease B, chicken ovalbumin, porcine thyroglobulin and desialylated thyroglobulin.

3.3. Multiple glycan structures

Fig. 5 shows the positive-ion ESI mass spectrum obtained for glycans released from chicken ovalbumin. The spectrum, which is dominated by sodiated glycan species $GlcNAc_nMan_3GlcNAc_2$ (n = 0, 1, 2),[1] is similar to one obtained previously using matrix-assisted laser desorption ionization (MALDI) [32]. The ion mobility separation and mobility-resolved MS/MS capabilities of the Synapt instrument give it great potential as a tool for investigating the structures and conformations of these glycans. If linkage isomers with different mobilities exist for a particular glycan we should be able to detect them by measuring an ATD. Likewise, information on conformers could be obtained if their mobilities are sufficiently different. Further information can be provided by measuring mass spectra for particular ATD features.

A review of oligosaccharide conformation studies by Wormald et al. [45] indicates that different conformations can arise through rotation about Man–Man linkages. The three dominant glycan peaks seen in our ovalbumin mass spectrum each have one Manα1–3Man link (.˙˙) and one Manα1–6Man link (˙˙.). The reviewed experimental and modeling studies indicate that the 1–3 link is flexible and that any different stable conformations present rapidly interconvert. The data available on the 1–6 link is less consistent. Analysis of existing crystal structures indicates that this link tends to take on three major and one minor conformation. NMR and modeling of a trisaccharide containing a Manα1–6Man link indicate two stable conformations, while modeling of $Man_9GlcNAc_2$ indicates the two Manα1–6Man links present each prefer a different single conformation.

The core glycan $Man_3GlcNAc_2$ should have only one linkage isomer as shown in Fig. 5 [46,47]. It is possible that this glycan has up to three significant conformers due to rotation around the Manα1–6Man link (since the Manα1–3Man link is not expected to take on distinct conformations). However, the differences in cross-section of the potential conformers might not be significant since only one sugar group is being moved by rotation about the 1–6 link. The ATD measured for the m/z 933 mass spectrum peak (Fig. 5) supports this contention since it has only a single, narrow feature. This result agrees well with the results of a DTIMS study of glycans released from ovalbumin by Plasencia et al. [26]. They find a single peak in their drift time distribution for permethylated, doubly sodiated $Man_3GlcNAc_2$.

For $GlcNAc_1Man_3GlcNAc_2$, there is the possibility of multiple linkage isomers depending on where the third GlcNAc group is added. Again there is the potential for conformers due to rotation about the Manα1–6Man link. These conformers may have significantly different cross-sections if the third GlcNAc group binds to the 1–6 branching Man group, since the 1–6 rotation would be moving this capping GlcNAc group. The ATD for the m/z 1136 peak is shown in Fig. 5 and has two dominant features.

[1] The MALDI study showed that some of the glycans observed in the ovalbumin sample actually arose from co-purifying glycoproteins and are not present in ovalbumin itself.

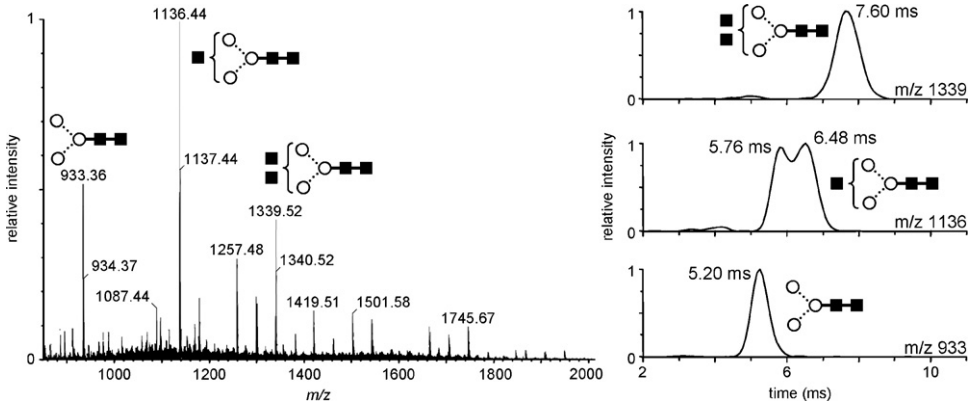

Fig. 5. Positive-ion mass spectrum obtained for glycans released from chicken ovalbumin using the Synapt instrument. The peaks for sodiated $GlcNAc_nMan_3GlcNAc_2$ ($n = 0$, 1, 2) are labeled with their respective structures (following key shown in Fig. 1). The corresponding TWIMS ATDs for these mass spectrum peaks are shown at right.

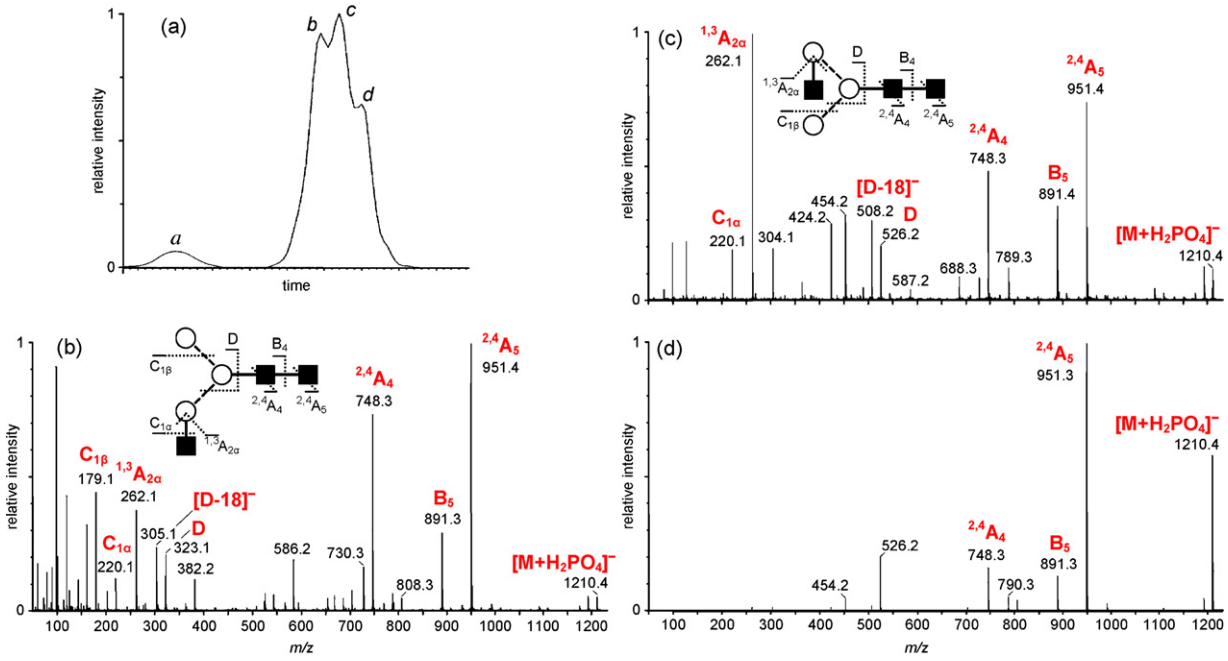

Fig. 6. (a) The negative ion TWIMS ATD for $GlcNAc_1Man_3GlcNAc_2$ (phosphate attachment) released from chicken ovalbumin. (b) The corresponding MS/MS spectrum for feature *b* in the ATD. (c) The corresponding MS/MS spectrum for feature *c* in the ATD. (d) The corresponding MS/MS spectrum for feature *d* in the ATD.

To help identify these two species, mobility-resolved MS/MS spectra (using the transfer region of the Synapt instrument) have been obtained for the two ATD features. Positive-ion (sodium attachment) spectra for the two ATD features (data not shown)[2] did exhibit some differences. In particular, differences in the relative intensities of peaks at *m/z* 388.2 corresponding to a sodiated ManGlcNAc group and *m/z* 933.4 corresponding to the loss of a single GlcNAc group would suggest different linkage isomers. However, the positive-ion data alone was not enough to identify the species associated with the two ATD features. The ATD measured for the $GlcNAc_1Man_3GlcNAc_2$ peak in negative ion mode (phosphate attachment) is shown in Fig. 6a and also has multiple features. The small peak at shortest arrival times (labeled *a*) is attributed to the doubly charged glycan dimer. The MS/MS spectra for each of the other three features (attributed to singly charge monomers) are shown in Fig. 6b–d and are notated using the carbohydrate nomenclature introduced by Domon and Costello [48].

The negative ion MS/MS data allow for the unambiguous determination of the structures corresponding to the two dominant ATD features as linkage isomers. The mass spectrum obtained for the ATD feature labeled *b* is shown in Fig. 6b. It has peaks at *m/z* 323 and 305, which can be assigned as the D (formal loss of the chitobiose core and 3-antenna) and D-18 fragments, respectively, from the isomer with the capping GlcNAc group bound to the Man group of the 1–3 branch [49]. The $^{1,3}A_{2\alpha}$ fragment at *m/z* 262 in the spectrum is consistent with this capping GlcNAc group being bound by a β1–2 linkage as shown in the figure (although 1–3, 1–4 and 1–6 linkages are possible) [50]. The mass spectrum for the ATD feature labeled *c* (Fig. 6c) has peaks at *m/z* 526 and 508. These D and D-18 fragment masses correspond to the isomer with the capping GlcNAc group bound to the Man group of the 1–6 branch, again consistent with a β1–2 linkage as indicated by the $^{1,3}A_{2\alpha}$ fragment at *m/z* 262.

A third, less intense feature in the negative ion ATD is observed at even longer arrival times. The MS/MS spectrum for this feature (labeled *d*) is shown in Fig. 6d and also exhibits peaks at *m/z* 526 and 508 indicating a 1–6 linkage isomer. This ATD feature could correspond to a conformer of the same 1–6 isomer already assigned to

[2] Data can be obtained by request from the authors.

Table 3
Experimental and theoretical results for penta- and hexasaccharides.

Oligosaccharide	DTIMS	Theory	TWIMS	
	Cross-section (Å^2)[a]	Cross-section (Å^2)	Arrival time (ms)	Est. cross-section (Å^2)[b]
[BP-S+Na]$^+$	185	186	3.20	185[c]
[iso-BP-S+Na]$^+$	185	190	3.20	185
[LNFP I+Na]$^+$	196	194	3.65	196
[LNFP V+Na]$^+$	194	196	3.51	193
[LNDFH I+Na]$^+$	217	216	4.50	217
[LNDFH II+Na]$^+$	214	217	4.28	211
[LNFP I+H]$^+$	185, 201	–	3.15, 3.87	184, 201
[LNFP V+H]$^+$	195	–	3.47	191

[a] Precision of cross-section values is smaller than ±2%.
[b] Cross-sections estimated from calibration with a precision of ±2%.
[c] [BP-S+Na]$^+$ used for cross-section calibration correction.

feature *c*, but the possibility of it corresponding to another 1–6 isomer could not be ruled out. Plasencia et al. [26] found four features in the drift time distribution for permethylated, doubly sodiated $Man_3GlcNAc_3$ with associated cross-sections ranging from approximately 292–328 Å^2.

For $GlcNAc_2Man_3GlcNAc_2$, there is again the possibility of linkage isomers as well as conformers. As shown in Fig. 5, the mass spectrum peak at *m*/*z* 1339 gives an ATD with a single feature centered around 7.60 ms. While this ATD feature is broader than that obtained for $Man_3GlcNAc_2$, an increase in the spread of arrival times is expected due to the later average arrival time of $GlcNAc_2Man_3GlcNAc_2$ and does not necessarily indicate the presence of multiple isomers or conformations. Plasencia et al. [26] also found only one feature in their drift time distribution for the permethylated, doubly sodiated version of this glycan. MALDI MS experiments [32] have suggested that there are two linkage isomers possible for this species with a GlcNAc residue bisecting the trimannose subunit and another bound to either the Manα1–3Man or Manα1–6Man branch, while an NMR study [31] finds only the first isomer. However, our negative ion MS/MS data for this species (not shown; see footnote 2) reveals no evidence for the bisecting GlcNAc residue [51]. One linkage isomer with a GlcNAc residue bound to the 1–3 branch and another to the 1–6 branch would be in better agreement with our observation of a single-peak ATD and the corresponding MS/MS results.

3.4. Comparison of the TWIMS and DTIMS methods

The measurement of absolute cross-sections is currently impossible using the TWIMS approach due to the very complex path the ions take as they traverse the mobility separator. TWIMS results can however be successfully calibrated against cross-sections of compounds measured in a DTIMS device. The resulting estimated cross-sections have been shown to be in good agreement with those measured using the established drift tube approach [16–19]. Here we compare values measured using DTIMS to those estimated using TWIMS for a series of oligosaccharides: BP-S and iso-BP-S; LNFP I and LNFP V; and finally LNDFH I and LNDFH II (Table 1).

All of these systems have been examined using the DTIMS instrument at UC Santa Barbara [33]. In each instance a strong sodiated parent ion was present in the mass spectrum, and for each of these cases a single symmetric ATD was observed (data not shown; see footnote 2). Experimental cross-sections determined in each case are listed in Table 3. Molecular modeling calculations revealed a single family of low-energy structures for each oligosaccharide. Representative structures, with the experimentally obtained cross-sections, are shown in Fig. 7 along with the corresponding average theoretical cross-sections for each family of structures. The theoretical cross-sections are also listed in Table 3. Several aspects of

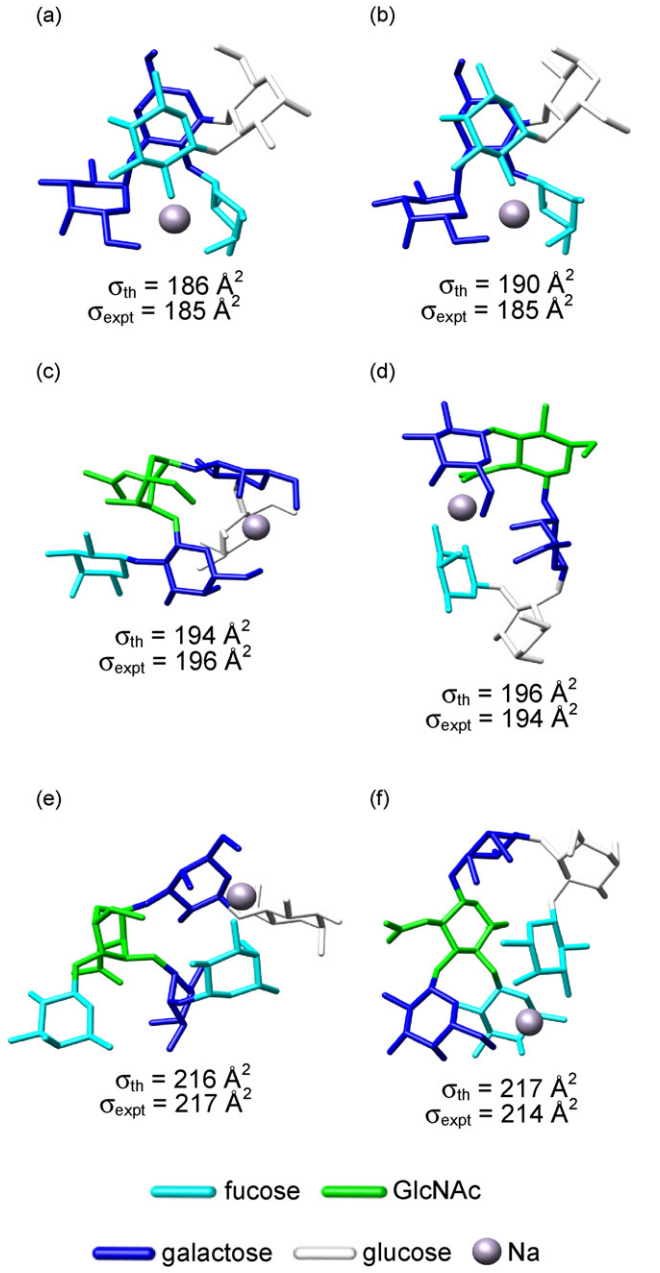

Fig. 7. Typical low-energy structures for sodiated (a) BP-S, (b) iso-BP-S, (c) LNFP I, (d) LNFP V, (e) LNDFH I and (f) LNDFH II determined by molecular dynamics calculations. The corresponding theoretical (σ_{th}) and experimental (σ_{expt}) cross-sections are also given for each oligosaccharide.

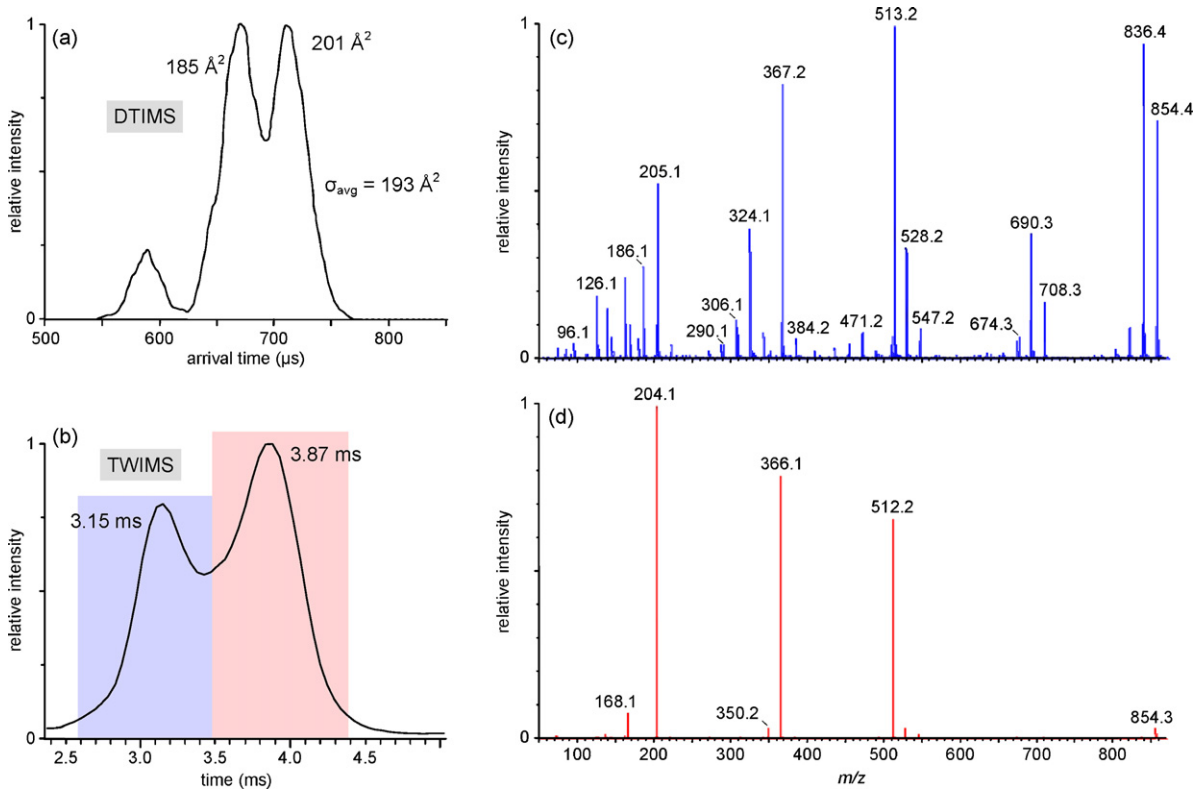

Fig. 8. ATDs for [LNFP I+H]$^+$ obtained using (a) DTIMS and (b) TWIMS and the tandem mass spectra of the (c) early and (d) late TWIMS ATD peaks.

these results deserve comment. First, there is excellent agreement between experiment and theory in all cases. The Na^+ ions were randomly placed on the molecules during simulated annealing runs and the same families of low-energy structures always emerged. Second, the BP-S and iso-BP-S structures observed are very similar, consistent with the identical experimental cross-sections. The other two sets of sodiated isomers have quite different structures yet they also have nearly identical cross-sections. This example provides a caution that the observation of very similar cross-sections does not necessarily imply the presence of similar conformations.

This same set of six oligosaccharides was examined using the TWIMS device and arrival time distributions obtained (data not shown; see footnote 2). The corresponding average arrival times are given in Table 3. Essentially identical arrival times were obtained for sodiated BP-S and iso-BP-S. Sodiated LNFP I and LNFP V also have very similar arrival times, and to a lesser extent, so do LNDFH I and II. It has been shown that the TWIMS device can be calibrated using cross-sections measured with a DTIMS instrument. It is important that calibration is carried out under identical TWIMS experimental conditions and using DTIMS calibration values that bracket the arrival times of interest [20]. The calibration method has been described in detail elsewhere [19] and entails comparing corrected effective TWIMS drift times to DTIMS cross-sections. The technique has been developed using a thorough set of DTIMS peptide cross-sections measured by Clemmer and coworkers [52]. The TWIMS cross-sections for the six oligosaccharides derived by this method were found to have a small linear offset from the corresponding DTIMS cross-sections reported here. For this reason, the TWIMS estimated cross-sections were corrected to the [BP-S+Na]$^+$ DTIMS cross-section to ensure consistency of comparison. These corrected TWIMS cross-sections are given in Table 3 along with the absolute cross-sections measured using DTIMS, the cross-sections derived from the molecular modeling structures and the arrival times from TWIMS.

The LNFP I and LNFP V systems have significant protonated parent peaks, in addition to the sodiated peaks seen for the other species. It should be noted the protonated peak in the mass spectrum of the DTIMS instrument was quite weak while the same peak was quite strong on the TWIMS instrument. The differences in spray methods and sampling, together with intrinsic sensitivity differences could account for this observation. While the ATDs for all the sodiated oligosaccharides and protonated LNFP V have just a single peak, the protonated LNFP I ATD has an additional feature as shown by both the DTIMS and TWIMS approaches (Fig. 8a and b). The corresponding DTIMS cross-sections for protonated LNFP I and V are given in Table 3 along with the TWIMS arrival times and estimated cross-sections, which agree well with the DTIMS values. The additional ATD feature for protonated LNFP I was initially thought to represent another conformer. Using the capability of the Synapt to obtain MS/MS data on mobility-separated compounds, MS/MS spectra were obtained in the transfer region for both ATD features. The results are given in Fig. 8c and d, which show product ion spectra of m/z 854 for both species. The mass spectrum for the longer-time ATD feature (Fig. 8d) is consistent with the simple fragmentation pattern expected for oligosaccharides in positive-ion mode and is similar to a positive-ion ESI mass spectrum obtained by Levin et al. [28]. The mass spectrum for the earlier ATD feature (Fig. 8c) has a much more complicated fragmentation pattern and is unlikely to be a result of a second conformation of LNFP I but rather an isomer or some other impurity. Unlike our bimodal ATD, the LNFP I differential mobility spectrum measured by Levin and coworkers has only one peak.

4. Conclusions

The ion mobility separation characteristics of the TWIMS device have been shown to be similar to the DTIMS device, although

the theoretical relationship between measured arrival times and mobility has not yet been established for the traveling wave technique. Previous work has indicated that mobility calibration of the TWIMS is possible using species of known collision cross-section [16–19]. This method has been successfully applied during this study. While the resolving power of the TWIMS is not as high as some DTIMS systems the separation capability is valuable for reducing mass spectral complexity, as shown for the complex released glycans. A particular advantage of the Synapt instrument over most DTIMS configurations is that the radial ion confinement in the mobility separator increases the overall instrument sensitivity, allowing investigations on analytically significant (fmol) levels of sample. This work illustrates that the TWIMS device provides rapid, sensitive and information-rich experimental data for the analysis of complex mixtures of glycans. The arrival times obtained are reproducible and independent of the source of the glycan. Some isomeric glycans can be separated and characterized using MS/MS experiments in favorable circumstances. The TWIMS device shows significant promise for screening complex glycan samples and for many other analytical applications in the characterization of biological systems.

Acknowledgments

The support of the Department of Food and Rural Affairs, UK, is gratefully acknowledged (JHS and MTB) as is the National Science Foundation, USA (MTB) and the Oxford Glycobiology Institute (DJH).

References

[1] R.A. Dwek, Chem. Rev. 96 (1996) 683–720.
[2] D.J. Harvey, Proteomics 1 (2001) 311–328.
[3] J.K.C. Ma, P.M.W. Drake, P. Christou, Nat. Rev. Genet. 4 (2003) 794–805.
[4] J. Gidden, A. Ferzoco, E.S. Baker, M.T. Bowers, J. Am. Chem. Soc. 126 (2004) 15132–15140.
[5] J. Gidden, E.S. Baker, A. Ferzoco, M.T. Bowers, Int. J. Mass Spectrom. 240 (2005) 183–193.
[6] E.S. Baker, S.L. Bernstein, M.T. Bowers, J. Am. Soc. Mass Spectrom. 16 (2005) 989–997.
[7] E.S. Baker, S.L. Bernstein, V. Gabelica, E. De Pauw, M.T. Bowers, Int. J. Mass Spectrom. 253 (2006) 225–237.
[8] V. Gabelica, E.S. Baker, M.P. Teulade-Fichou, E. De Pauw, M.T. Bowers, J. Am. Chem. Soc. 129 (2007) 895–904.
[9] S.L. Bernstein, T. Wyttenbach, A. Baumketner, J.-E. Shea, G. Bitan, D.B. Teplow, M.T. Bowers, J. Am. Chem. Soc. 127 (2005) 2075–2084.
[10] A. Baumketner, S.L. Bernstein, T. Wyttenbach, G. Bitan, D.B. Teplow, M.T. Bowers, J.-E. Shea, Protein Sci. 15 (2006) 420–428.
[11] S.L. Bernstein, N.F. Dupuis, N.D. Lazo, T. Wyttenbach, M.M. Condron, G. Bitan, D.B. Teplow, J.-E. Shea, B.T. Ruotolo, C.V. Robinson, M.T. Bowers, Nat. Chem. 1 (2009) 326–331.
[12] A.M. Last, C.V. Robinson, Curr. Opin. Chem. Biol. 3 (1999) 564–570.
[13] A.J.R. Heck, R.H.H. van den Heuvel, Mass Spectrom. Rev. 23 (2004) 368–389.
[14] K. Giles, S.D. Pringle, K.R. Worthington, D. Little, J.L. Wildgoose, R.H. Bateman, Rapid Commun. Mass Spectrom. 18 (2004) 2401–2414.
[15] S.D. Pringle, K. Giles, J.L. Wildgoose, J.P. Williams, S.E. Slade, K. Thalassinos, R.H. Bateman, M.T. Bowers, J.H. Scrivens, Int. J. Mass Spectrom. 261 (2007) 1–12.
[16] B.T. Ruotolo, K. Giles, I. Campuzano, A.M. Sandercock, R.H. Bateman, C.V. Robinson, Science 310 (2005) 1658–1661.
[17] J.P. Williams, J.H. Scrivens, Rapid Commun. Mass Spectrom. 22 (2008) 187–196.
[18] C.A. Scarff, K. Thalassinos, G.R. Hilton, J.H. Scrivens, Rapid Commun. Mass Spectrom. 22 (2008) 3297–3304.
[19] K. Thalassinos, M. Grabenauer, S.E. Slade, G.R. Hilton, M.T. Bowers, J.H. Scrivens, Anal. Chem. 81 (2009) 248–254.
[20] J.A. Leary, M.R. Schenauer, R. Stefanescu, A. Andaya, B.T. Ruotolo, C.V. Robinson, K. Thalassinos, J.H. Scrivens, M. Sokabe, J.W.B. Hershey, J. Am. Soc. Mass Spectrom 20 (2009) 1699–1706.
[21] S. Lee, T. Wyttenbach, M.T. Bowers, Int. J. Mass Spectrom. Ion Processes 167 (1997) 605–614.
[22] L. Jin, P.E. Barran, J.A. Deakin, M. Lyon, D. Uhrin, Phys. Chem. Chem. Phys. 7 (2005) 3464–3471.
[23] Y.S. Liu, D.E. Clemmer, Anal. Chem. 69 (1997) 2504–2509.
[24] D.S. Lee, C. Wu, H.H. Hill, J. Chromatogr. A 822 (1998) 1–9.
[25] B.H. Clowers, P. Dwivedi, W.E. Steiner, H.H. Hill, B. Bendiak, J. Am. Soc. Mass Spectrom. 16 (2005) 660–669.
[26] M.D. Plasencia, D. Isailovic, S.I. Merenbloom, Y. Mechref, D.E. Clemmer, J. Am. Soc. Mass Spectrom. 19 (2008) 1706–1715.
[27] P. Dwivedi, B. Bendiak, B.H. Clowers, H.H. Hill, J. Am. Soc. Mass Spectrom. 18 (2007) 1163–1175.
[28] D.S. Levin, P. Vouros, R.A. Miller, E.G. Nazarov, J. Am. Soc. Mass Spectrom. 18 (2007) 502–511.
[29] P. de Waard, A. Koorevaar, J.P. Kamerling, J.F.G. Vliegenthart, J. Biol. Chem. 266 (1991) 4237–4243.
[30] D.T. Fu, L. Chen, R.A. O'Neill, Carbohydr. Res. 261 (1994) 173–186.
[31] M.L.C. Da Silva, H.J. Stubbs, T. Tamura, K.G. Rice, Arch. Biochem. Biophys. 318 (1995) 465–475.
[32] D.J. Harvey, D.R. Wing, B. Kuster, I.B.H. Wilson, J. Am. Soc. Mass Spectrom. 11 (2000) 564–571.
[33] T. Wyttenbach, P.R. Kemper, M.T. Bowers, Int. J. Mass Spectrom. 212 (2001) 13–23.
[34] E.A. Mason, E.W. McDaniel, Transport Properties of Ions in Gases, Wiley, New York, 1988.
[35] T. Patel, J. Bruce, A. Merry, C. Bigge, M. Wormald, A. Jaques, R. Parekh, Biochemistry 32 (1993) 679–693.
[36] D.A. Case, T.A. Darden, T.E. Cheatham, C.L. Simmerling, J. Wang, R.E. Duke, R. Luo, K.M. Merz, B. Wang, D.A. Pearlman, M. Crowley, S. Brozell, V. Tsui, H. Gohlke, J. Mongan, V. Hornak, G. Cui, P. Beroza, C. Schafmeister, J.W. Caldwell, W.S. Ross, P.A. Kollman, AMBER 8, University of California, San Francisco, 2004.
[37] Hyperchem 7.0., Hypercube, Inc., Gainesville, FL, 2002.
[38] M.J. Frisch, G.W. Trucks, H.B. Schlegel, G.E. Scuseria, M.A. Robb, J.R. Cheeseman, J.A. Montgomery, T. Vreven, K.N. Kudin, J.C. Burant, J.M. Millam, S.S. Iyengar, J. Tomasi, V. Barone, B. Mennucci, M. Cossi, G. Scalmani, N. Rega, G.A. Petersson, H. Nakatsuji, M. Hada, M. Ehara, K. Toyota, R. Fukuda, J. Hasegawa, M. Ishida, T. Nakajima, Y. Honda, O. Kitao, H. Nakai, M. Klene, X. Li, J.E. Knox, H.P. Hratchian, J.B. Cross, V. Bakken, C. Adamo, J. Jaramillo, R. Gomperts, R.E. Stratmann, O. Yazyev, A.J. Austin, R. Cammi, C. Pomelli, J.W. Ochterski, P.Y. Ayala, K. Morokuma, G.A. Voth, P. Salvador, J.J. Dannenberg, V.G. Zakrzewski, S. Dapprich, A.D. Daniels, M.C. Strain, O. Farkas, D.K. Malick, A.D. Rabuck, K. Raghavachari, J.B. Foresman, J.V. Ortiz, Q. Cui, A.G. Baboul, S. Clifford, J. Cioslowski, B.B. Stefanov, G. Liu, A. Liashenko, P. Piskorz, I. Komaromi, R.L. Martin, D.J. Fox, T. Keith, M.A. Al-Laham, C.Y. Peng, A. Nanayakkara, M. Challacombe, P.M.W. Gill, B. Johnson, W. Chen, M.W. Wong, C. Gonzalez, J.A. Pople, Gaussian 03, Revision C.02., Gaussian, Inc., Wallingford, CT, 2004.
[39] M.F. Mesleh, J.M. Hunter, A.A. Shvartsburg, G.C. Schatz, M.F. Jarrold, J. Phys. Chem. 100 (1996) 16082–16086.
[40] A.A. Shvartsburg, M.F. Jarrold, Chem. Phys. Lett. 261 (1996) 86–91.
[41] E.F. Pettersen, T.D. Goddard, C.C. Huang, G.S. Couch, D.M. Greenblatt, E.C. Meng, T.E. Ferrin, J. Comput. Chem. 25 (2004) 1605–1612.
[42] G.R. Guile, P.M. Rudd, D.R. Wing, S.B. Prime, R.A. Dwek, Anal. Biochem. 240 (1996) 210–226.
[43] D.J. Harvey, A.H. Merry, L. Royle, M. Campbell, R.A. Dwek, P.M. Rudd, Proteomics 9 (2009) 3796–3801.
[44] D.J. Harvey, J. Mass Spectrom. 35 (2000) 1178–1190.
[45] M.R. Wormald, A.J. Petrescu, Y.L. Pao, A. Glithero, T. Elliott, R.A. Dwek, Chem. Rev. 102 (2002) 371–386.
[46] K. Yamashita, J.P. Kamerling, A. Kobata, J. Biol. Chem. 258 (1983) 3099–3106.
[47] H. Egge, J. Peterkatalinic, J. Pazparente, G. Strecker, J. Montreuil, B. Fournet, FEBS Lett. 156 (1983) 357–362.
[48] B. Domon, C.E. Costello, Glycoconjug. J. 5 (1988) 397–409.
[49] D.J. Harvey, L. Royle, C.M. Radcliffe, P.M. Rudd, R.A. Dwek, Anal. Biochem. 376 (2008) 44–60.
[50] D.J. Harvey, J. Am. Soc. Mass Spectrom. 16 (2005) 631–646.
[51] D.J. Harvey, J. Am. Soc. Mass Spectrom. 16 (2005) 647–659.
[52] S.J. Valentine, A.E. Counterman, D.E. Clemmer, J. Am. Soc. Mass Spectrom. 10 (1999) 1188–1211.